6 Upper stratosphere to thermosphere effects and H₂O transport in the deep Brewer-Dobson branch

Lead authors	Corwin Wright
	Jia Yue
Co-authors	Neil Hindley
	Jinhou Lei
	Luis F. Millán
	David Themens
	Sandra Wallis
	Wandi Yu
Contributing authors	Ewa M. Bednarz
	Eric Fleming
	Ruoxi Li
	David Plummer
	Simone Tilmes
	Xinyue Wang
	Jun Zhang
	Yunqian Zhu
	Zhihong Zhuo

Key points

- The Hunga eruption produced short-term gravity wave and Lamb wave responses unprecedented in the observational record which traversed the world for several days, reaching the top of the terrestrial atmosphere and with major impacts as high as the ionosphere-thermosphere system.

- Major ionospheric impacts were recorded which significantly advanced our understanding of TIDs, including some of the largest amplitude lower atmospherically-driven TIDs ever observed. Neutral atmospheric impacts were similarly dramatic and have significantly advanced our knowledge of wave propagation and dynamics in the stratosphere and above.

- Water vapour was initially injected into the stratosphere and by May 2023 was subsequently transported up to the mesosphere where a large fraction remains at time of writing. The vapour has been distributed globally since August 2023, and has had significant impacts on the dynamical and chemical state of the mesosphere.

- Models reproduce the observed water and ozone effects well. Mesospheric water vapour increased by ~3-4 Tg in 2023 via vertical transport from the stratosphere, while HOx chemistry led to depletion of mesospheric ozone. The resulting reduction in ozone shortwave heating and water vapour cooling led to a >1K temperature decrease in global mean mesospheric temperatures. Models however had much more difficulty reproducing the observed dynamical and temperature effects induced by stratospheric wind changes and gravity wave drag during 2022.

- Model simulations indicate that perturbations to mesospheric temperature, water vapour, and ozone concentrations are expected to persist beyond 2026. MLS observations substantiate model evidence that the maximum anomaly occurred in 2023, followed by a gradual decline. By 2027, the residual effects are likely to fall below statistical significance relative to climatological variability.

Contents

Preamble

This chapter describes the impact of the Hunga eruption on Earth's upper-middle and upper atmosphere, from the upper stratosphere to the thermosphere-ionosphere system. The explosion and plume triggered both direct and indirect chemical, radiative and dynamical impacts on all these layers, providing a dramatic natural experiment elucidating many key aspects of their structure and dynamics. In the initial hours after the eruption, Lamb waves and acoustic-gravity waves penetrated deep into the upper atmosphere and were observed propagating at global scales through the ionosphere and thermosphere. The eruption simultaneously injected large volumes of water vapour into the stratosphere, and the upward transport and radiative effects of this water proved to be the longest-term impact in these atmospheric layers: leading to mesospheric cooling and ozone depletion. Dynamically, it also led to record-breaking warming over the extratropical southern hemisphere and cooling throughout the rest of the mesosphere during boreal summer 2022. Climate models have been able to reproduce these chemical and dynamic effects of water vapour, but with varying degrees of success. Based on these models, we believe that the residual effects of this injected water vapour are likely to fall below statistical significance relative to climatological variability by 2027.

6.1 Introduction

Above the stratosphere lies the Earth's upper atmosphere, consisting of the mesosphere and thermosphere. Due to incoming solar UV radiation, part of the thermosphere is ionised, a region known as the ionosphere.

Air densities in the upper atmosphere are extremely low, and consequently are often treated as part of space - indeed, objects in LEO, including the international space station, actually fly within the thermosphere. Simultaneously, radio wave communications and GNSS navigation rely on the propagation of electromagnetic signals through the ionosphere. As such, it is important to characterise and quantify the variability of the upper atmosphere as driven by Earth system sources such as the Hunga eruption.

A highly unusual feature of the Hunga eruption was that it penetrated deep into the middle and upper layers of the atmosphere, with the initial plume reaching 58 km in height, an altitude above the stratopause at this time of year and location (Proud et al., 2022). At this altitude the explosion and plume triggered both

direct and indirect chemical, radiative and dynamical impacts on the middle and upper neutral atmosphere and on the charged ionosphere, which we discuss in this chapter.

Within the initial hours after the eruption, Lamb waves (Lamb, 1881) and acoustic-gravity waves penetrated deep into the upper atmosphere and were observed across the global ionosphere. These immediate effects, and their implications are discussed in Sections 6.2 and 6.3. The underlying mechanisms driving these thermospheric responses remain elusive and are an object of active research. We next consider the much longer timescale processes by which water vapour injected into the stratosphere reached the lower mesosphere, taking over a year to reach lower mesospheric altitudes via the slow progress of the global general circulation. This had concomitant impacts on the temperature structure and chemical composition of the upper atmosphere, which are discussed in Sections 6.4 and 6.5.

6.2 Short-term dynamical impacts on the middle atmosphere

As mentioned in Chapter 2, the initial eruption of Hunga triggered Lamb, acoustic and gravity waves which propagated in a period of hours from the surface to the upper thermosphere, coupling directly into the ionosphere (Wright et al., 2022; Matoza et al., 2022; Themens et al., 2022). Observations of these waves provide a dramatic demonstration of deep vertical coupling between atmospheric layers unique in the long-term satellite observational record, as well as a key scientific test for large parts of linear wave theory. In particular, this event represents the first time a Lamb wave has been observed in the middle and upper atmospheres by satellite.

6.2.1 Stratosphere and mesosphere

In the stratosphere and mesosphere, an extremely broad spectrum of waves was seen after the eruption, produced by generation mechanisms both immediate and also spread out over most of the day following the initial eruption.

The initial eruption immediately produced intense atmospheric waves which became visible in the stratospheric portion of the plume within 20 minutes of the eruption (Smart, 2022; Proud et al., 2022; Carr et al., 2022; Wright et al., 2022). The observed spectrum at these timescales was dominated by a single high-amplitude Lamb wave which propagated radially outwards from the eruptive centre with a phase

speed of ~318 m s^{-1}. This wave was present throughout the entire depth of the middle atmosphere. The Lamb wave rapidly propagated out of the plume but remained clearly visible in stratospheric radiance (i.e. emitted atmospheric radiant flux) measurements from a range of satellite platforms including AIRS, ATMS CIPS, CRIS, and IASI, and was tracked over a period of days as it propagated around the Earth multiple times (Ern et al., 2022; Wright et al., 2022; Lee et al., 2023; Zhou et al., 2023, Figure 6.1). During these multiple laps around the Earth, the wave showed no significant evidence of any dispersion. This 'primary' Lamb wave's propagation across the globe was almost entirely radial, but with deviations from a purely radial path consistent with the column-mean atmospheric state, large-scale winds and surface topography rather than the state at any specific height level (Inchin et al., 2023; Sepúlveda et al., 2023; Wright et al., 2022). At least two lower-amplitude Lamb waves were subsequently produced by later phases of the eruption, and were also observed propagating through the stratosphere at global scales (Wright et al., 2022). Along with the Lamb waves, a slower horizontal phase speed internal Pekeris wave, a resonance oscillation inherent to the Earth's atmosphere, was excited as a normal mode of the global atmosphere (Watanabe et al., 2022; Ohya et al., 2024).

The same initial eruptive burst that produced the first high-amplitude Lamb wave also produced internal gravity waves across a broad spectrum of horizontal wavelengths, all with extremely long vertical wavelengths of comparable depth to the homosphere (i.e. the layer of the atmosphere between the surface and 100 km where longer-lived atmospheric gases are well mixed; Liu et al., 2022; Ern et al., 2022; Wright et al., 2022). These waves propagated rapidly outwards at their upper-bound phase speed in a radial direction. On planetary scales, the waves separated out by horizontal wavelength as a result of fundamental physical limits on their horizontal phase speeds, which covered an extremely broad range from near-zero up to a "speed limit" of ~270 m s^{-1} (Wright et al., 2022). Within hours, a clear spatial gap was visible between the initial-burst Lamb waves and gravity waves, consistent with a theoretically-forbidden phase speed range between Lamb waves and gravity waves which had not previously been observed but which is consistent with linear wave theory (Figure 6.1). Gravity waves were subsequently generated by the plume over a period of hours, which propagated visibly across the entire Pacific basin but

at slower speeds than the theoretical limit of the initial gravity wave burst emitted along with the initial Lamb wave. Despite their large amplitudes, these waves transferred very little momentum to the background, and no short-term impact was seen on stratospheric dynamics due to their passage (Wright et al., 2022). No significant evidence of these waves being refracted by the large-scale background winds was seen, likely due to their very high phase speed.

Globe-spanning gravity and Lamb waves are completely unprecedented in the satellite record from any source. For comparison, gravity waves generated by large-scale hurricanes typically dissipate within a few thousand kilometres at most (Wright, 2019), while waves refracted into the polar night jet streams travel shorter distances than this. The lack of observations of this type of wave could partly be due to the limited length of the data record, since satellite instruments of the types used to study the Hunga-produced atmospheric waves by e.g. Ern et al. (2022), Matoza et al. (2022), Wright et al. (2022) and Lee et al. (2023) have only been available since the 2000s, i.e. well after the 1991 Pinatubo eruption.

Ground-based data records of atmospheric waves observed by airglow imagers, radar and lidar extend back some decades with no evidence of similar wave activity. The lack of an atmospheric dataset record of such events is also consistent with long-term surface pressure measurements, which would be able to measure the surface aspect of a Lamb wave of the magnitude seen after the Hunga eruption. Such features have previously been seen in ionospheric data, e.g. by Liu et al. (1982) for the 1980 Mt. St. Helens eruption.

Smaller convective waves of the type seen at stratospheric and mesospheric levels in the plume have however been seen after previous volcanic eruptions, consistent with our broader knowledge of convective gravity wave physics. In particular, previous studies have discussed internal gravity waves seen in airglow after the smaller-magnitude La Soufriere (2021, VEI 4) and Calbuco (2015, VEI 4) eruptions (Miller et al., 2015; Yue et al., 2022). Retrospective analysis of AVHRR radiances measured during the 1991 eruption of Pinatubo carried out after the Hunga eruption also shows evidence of gravity wave phase fronts in the plume (Wright et al., 2022). It is thus likely that smaller gravity waves are generated in the plumes of many large volcanic eruptions, albeit with a much smaller magnitude and propagation range relative to those observed after the 2022 Hunga eruption (e.g. Wright
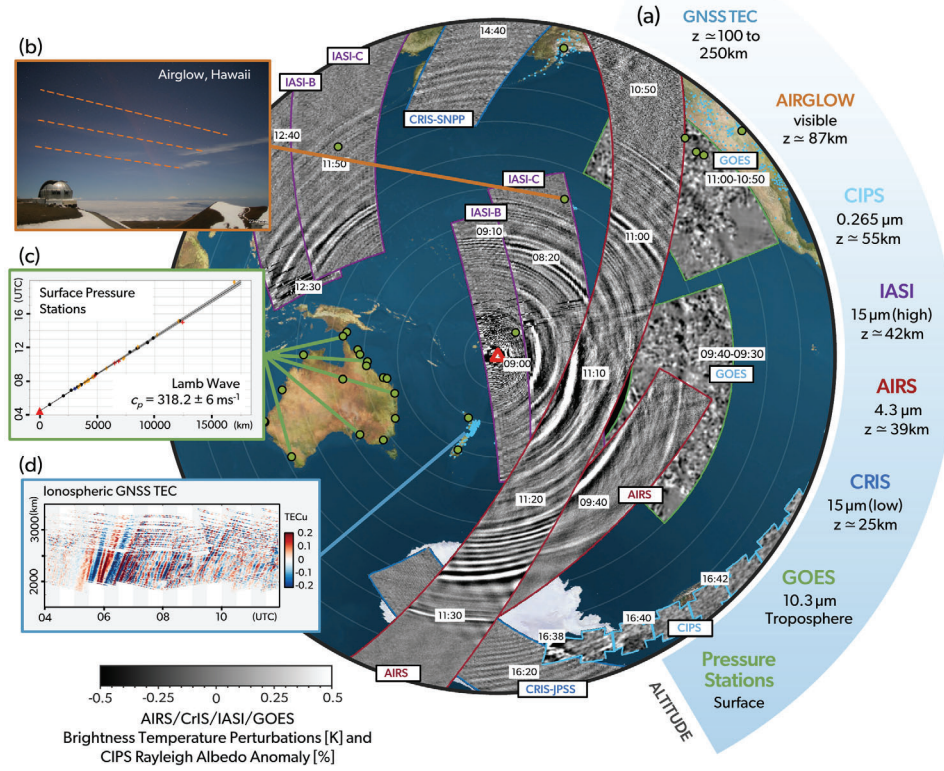
Figure 6.1: *Atmospheric waves from the initial eruption observed across the Pacific Ocean by a range of instruments. Coloured outlines of swaths identify each instrument using the key at right, with observation times overlaid in white boxes. Reproduced with minor modifications from Wright et al. (2022).*

et al., 2022). However, in contrast to Hunga, such wave activity seen in the stratosphere after previous 20th and 21st century eruptions has been significantly more spatially-localised, lower-amplitude and of shorter duration, and the waves have not propagated long distances from the initial eruptive source (e.g. Yue et al., 2022).

6.2.2 Impacts on the thermosphere

The Hunga-triggered atmospheric disturbances also reached above the middle atmosphere, extending as high as the upper thermosphere (Li et al., 2023a; Wright et al., 2022). These disturbances in turn coupled into the overlapping charged ionosphere, and we discuss these ionospheric impacts separately in Section 6.3 below.

In the neutral (i.e. uncharged) thermosphere, global-scale variations in wind and temperature associated with the Hunga eruption were captured by ICON-MIGHTI and GOLD (Aryal et al., 2023; Harding et al., 2022) and by methods including the MANGO network (Inchin et al., 2023) and hydroxyl airglow (Wright et al., 2022). Additionally, eruption-induced meso-

spheric local wind changes were also detected by ground-based meteor radars (Poblet et al., 2023; Stober et al., 2023). Furthermore, Li et al. (2023b) derived thermospheric mass densities from GRACE-FO (Landerer et al., 2020) satellite accelerometer data, and demonstrated the existence of globally-propagating post-eruption thermospheric waves and subsequent mass density redistributions. The underlying mechanisms driving these thermospheric responses remain elusive and are an object of active research.

Various physical models have been employed to elucidate the upper atmospheric reaction to the eruption (Huba et al., 2023; Liu et al., 2023; Wu et al., 2023; Vadas et al., 2023a; Vadas et al., 2023b). Liu et al. (2023) used WACCM-X to replicate the global propagation of the L0 and L1 modes (i.e. two leading-order modes) of the Lamb waves emitted in the initial eruption, and demonstrated consistency with ICON-MIGHTI wind observations in terms of wind perturbations, wavefront tilting, and propagation speeds. Moreover, a large observed wind perturbation along the northwest coast of South America coincided with the simulated L1 mode (Poblet et al., 2023; Chau et al., 2024).

Studies such as those of Vadas et al. (2023a) and Stober et al. (2023) and Stober et al. (2024) have instead argued for a significant role for 'secondary' gravity waves (i.e. gravity waves triggered within the atmospheric column due to the breakdown of other 'primary' waves from near-surface sources) instead of Lamb waves in generating the observed large-scale fluctuations in wind. Vadas et al. (2023a) employed the MESORAC to compute primary gravity waves, subsequently utilising the associated local body forces as input into the HIAMCM to simulate secondary gravity waves, with results aligning with far-field wind observations. However, the scarcity of thermospheric measurements makes it challenging to elucidate the primary energy transformation process from the eruption epicentre to a global scale, and the exact transfer mechanism thus remains an open question.

6.3 Impacts on the ionosphere

Waves generated in the thermosphere by the Hunga eruption generated a wide range of different waves in the ionosphere and produced a global-scale ionospheric response (Themens et al., 2022; Wright et al., 2022; Zhang et al., 2022). Ionospheric responses to the eruption included gravity wave-induced MSTIDs with wavelengths of tens to hundreds of kilometres and LSTIDs with wavelengths greater than a thousand kilometres, strong electrical currents, magnetically conjugate disturbances, and a deep ionospheric depletion near the location of the eruption.

MSTIDs were among the first documented features of the event, where waves in the ionosphere of similar scale and propagation characteristics to the gravity waves generated in the stratosphere and mesosphere were observed in ionospheric observations of the column integrated plasma density of the ionosphere, i.e. TEC (Themens et al., 2022; Wright et al., 2022; Zhang et al., 2022). MSTIDs were observed globally (Themens et al., 2022) across all continents (e.g., Asia: Li et al., 2023b; Europe: Verhulst et al., 2022; North America: Zhang et al., 2022; South America: Takahashi et al., 2023; Pacheco et al., 2024; Africa: Themens et al., 2022), and for several days following the eruption (Zhang et al., 2022).

The exact nature of the coupling mechanisms through which the gravity waves in the lower atmosphere generated waves in the thermosphere, and correspondingly in the ionosphere, is still a subject of extensive research. Themens et al. (2022) and Zhang et al. (2022) observed these TIDs propagating globally. However, studies such as Vadas et al. (2023a) and Vadas et al. (2023b) and Stober et al. (2023) and Stober et al. (2024) argue through both modelling and ionospheric and mesospheric observations, that these TIDs, as with the Lamb waves discussed above, are the result of secondary gravity waves generated by wave breaking in the mesosphere. Meanwhile, other modelling studies by (Wu et al., 2023; Liu et al., 2023; Miyoshi and Shinagawa, 2023) suggest Lamb waves as their origin, Ohya et al. (2024) discuss their relationship to Pekeris waves, and Inchin et al. (2023) highlight the diversity of potential mechanisms and the importance of the Hunga event as a natural laboratory for expanding our understanding of wave source processes, atmospheric gravity wave (AGW) propagation, and coupling across scales. To this end, the TIDs generated by the Hunga eruption are some of the most broadly modelled ionospheric responses to lower atmospheric external forcing, with studies carried out using WACCM-X (Liu et al., 2023), GAIA (Miyoshi and Shinagawa, 2023), grid-refined TIE-GCM (Wu et al., 2023), and SAMI3 coupled to HIAMCM and MESORAC (Huba et al., 2023; Vadas et al., 2023a; Vadas et al., 2023b).

In addition to MSTIDs, LSTIDs were also generated by the eruption and were observed both locally within a few thousand kilometres of the eruption (Themens et al., 2022; Wright et al., 2022; Zhang et al., 2022) and globally over North and South America (Figueiredo et al., 2023; Vadas et al., 2023b). Near the eruption, these LSTIDs had amplitudes of 3-8 TEC Units (TECU) depending on detrending scale and processing method (Zhang et al., 2022), making them some of the largest-amplitude lower atmospherically-driven TIDs ever observed. Ionosonde observations of the bottomside ionosphere also show LSTID variations in peak electron density of greater than 50% and variations in the height of the ionospheric peak by 100 to 150 km (Vadas et al., 2023b). Modelling by Vadas et al. (2023b) demonstrated good agreement with observations and suggests that these LSTIDs were directly caused by secondary gravity waves induced by the eruptive primary wave.

Waves generated locally by the eruption were also found to generate TIDs in the magnetically conjugate hemisphere, i.e. on the other end of the magnetic field lines where primary TIDs were observed, both broadly over Asia (Shinbori et al., 2022; Lin et al., 2022) and directly under the eruption's magnetic conjugate footprint near Hawaii (Themens et al., 2022). This resulted in TIDs appearing at these conjugate points nearly coincidently with their hemispheric counter-

parts and, in some cases, interfering with later arriving TIDs that propagate directly from the eruption (Themens et al., 2022).

In addition to the TIDs generated by this event, the eruption generated unprecedented electric field disturbances in the vicinity of the eruption (Gasque et al., 2022; Harding et al., 2022; Le et al., 2022; Yamazaki et al., 2022), observed through in situ satellite measurements by the Swarm satellites and by ground-based magnetometer observations. The large-scale ionospheric response also included the generation of a large ionospheric "hole" of up to 13 TECU near the eruption location that did not recover before sunset (Astafyeva et al., 2022; He et al., 2023; Choi et al., 2023). This plasma density depletion was coincident with a corresponding large thermospheric density depletion, but the relationship between these is still not fully understood (Li et al., 2023a). The work of Zettergren et al. (2017) would suggest that the ionospheric depletion may be the result of nonlinear, dissipating acoustic waves following the initial shock. While this work strongly correlates with the impact observed for this event, more modelling of this type for this event is necessary in order to conclusively attribute this mechanism as the cause of the depletion. This is particularly important given that Zettergren et al. (2017) only modelled waves generated through surface displacements, while this event also included substantial water vapour deposition in the stratosphere and lower mesosphere which could significantly change the nature and source of the waves at play in this case. There remain considerable opportunities for the modelling of the observed response to this event.

The TIDs and electric field disturbances generated by this event are observed (Aa et al., 2022a; Aa et al., 2022b; Carter et al., 2023; Rajesh et al., 2022; Pacheco et al., 2024; Shinbori et al., 2023) and modelled (Huba et al., 2023) to have seeded equatorial plasma bubbles of unprecedented scale (exceeding altitudes of ~1900 km), depth (exceeding 43 TECU), and resulting in GNSS positioning challenges over Australia (Carter et al., 2023).

The event also stimulated considerable interest in the use of the resulting ionospheric waves for monitoring and, potentially, warning against ensuing tsunamis (Han et al., 2023; Pradipta et al., 2023; Maletckii and Astafyeva, 2022). However, there remains considerable research required in order to translate these observations into actionable warnings or measurement techniques, as the relationship between ionospheric wave characteristics and the properties of tsunami

waves remains uncertain (Ravanelli et al., 2023). This event has served as a natural laboratory in which to test and push the boundaries of our understanding of TIDs, their generation, and atmosphere-ionosphere coupling as a whole. The collective observations and simulations of the ionospheric response to this eruption are unprecedented compared to any past seismological or meteorological events occurring in the lower atmosphere and the magnitude of the signature, observed the world over, made this event unique. This allowed this event to stimulate extensive discussions in the community on the nature of atmosphere-ionosphere coupling, with still-unknown outcomes and untested hypotheses, particularly related to the role of nonlinear and higher order wave dynamics in the observed ionospheric response, as well as related to the internal processes within TIDs (Klenzing et al., 2025). In the coming years, we may yet see studies of this event substantially advance our capacity to develop early warning systems for tsunamis, build better models of the ionosphere, and solve many of our outstanding questions related to how waves in the lower atmosphere drive ionospheric dynamics.

6.4 Water vapour transport in the middle and upper atmosphere

We now consider the effects of the eruption on middle- and upper-atmospheric water vapour, arguably the largest impact of Hunga on this large region of the neutral atmosphere. Evolution of the water vapor plume in the stratosphere is thoroughly discussed in Chapters 2 and 3, and we refer the reader there for further contextual details.

The initial eruption injected water vapour across the whole depth of the stratosphere, reaching directly into the lower mesosphere (Millán et al., 2022; Proud et al., 2022). The plume rapidly descended from this absolute peak, likely due to longwave radiative cooling of its upper part (Sellitto et al., 2022; Niemeier et al., 2023), and the majority settled between 20-40 hPa (approximately 20-30 km), i.e. in the lower stratosphere, where it remained for several months (Millán et al., 2022; Legras et al., 2022; Niemeier et al., 2023). Thus, the initial injection did not affect the mesosphere.

Hunga-hydrated air re-entered the mesosphere 16 months after the eruption in May 2023 (Figure 6.2a,j), where it split into northward and southward branches, consistent with transport via the climatological Brewer Dobson Circulation. By June 2023 (Figure 6.2b), it reached into the northern tropical lower mesosphere, and by August 2023 (Figure 6.2c)

blanketed the entire lower mesosphere in the southern hemisphere and most of the northern hemisphere. By the beginning of 2024, i.e. two years after the eruption (Figure 6.2f), the vapour was almost entirely absent from the tropical stratosphere, displaced by dryer air entering through the tropical tropopause. At higher altitudes however, the vapour had expanded through much of the lower mesosphere, reaching maximal altitudes of 0.07 hPa at southern high latitudes (Nedoluha et al., 2024; Millán et al., 2024). In the following months, i.e. the beginning and middle of 2024 (Figures 6.2g–6.2i), the additional vapour oscillated between the Northern and Southern Hemispheres in response to the mesospheric general circulation.

Figure 6.3a,b contextualises the additional water vapour introduced into the middle and upper atmosphere by showing the observed annual cycle of near-global (82°S-82°N) mesospheric water vapour mass over the 20+ years of the Microwave Limb Sounder (MLS) record, with post-2022 data highlighted. Independently of the Hunga eruption, we see elevated water vapour mass in late 2022 and early 2023 which arises partly due to dynamical conditions that enhanced methane oxidation and increased water vapour (Nedoluha et al., 2023). Despite this, the impact of the Hunga eruption is clearly visible from May 2023, when the mesospheric water vapour burden jumped from 23 to 26 Tg in just 3 months, up to 4 Tg above climatological values. These anomalously moist mesospheric conditions led in turn to an unprecedentedly low global mesospheric ozone burden beginning around August 2023 and lasting until June 2024 (Figure 6.3c,d), which may have been driven, at least in part, by the impact of the additional humidity on the HOx catalytic cycles (e.g., Brasseur and Solomon, 2005; Randel et al., 2024). The evolution of global mid-mesospheric (0.1 hPa) temperatures has remained within the climatological range, except in October 2023 and a few days in August 2023 and February 2024 (Figure 6.3e,f), when the values in the MLS record were marginally cooler by about 1 K than in previous years. Randel et al. (2024) argue that this cooling was mostly caused by the low ozone burden associated with HOx chemistry from the elevated water vapor values and the water vapour related cooling.

PMCs or noctilucent clouds form in the polar mesopause summer when ambient temperatures drop below 150 K and water vapour is saturated. The first sighting of noctilucent clouds was reported 2 years after the 1883 Krakatau volcanic eruption (VEI 6)

(Leslie, 1885). After the 2022 Hunga eruption, no clear response in PMCs occurrence frequency was detected from OMPS-LP measurements during the 2023/2024 and 2024 season. Although a 1 ppmv water vapour anomaly reached the polar summer mesopause in the Northern Hemisphere during 2024, ice particle formation may have been hindered by anomalous warming (Wallis et al., 2025).

6.5 Modelling of long-term middle-atmospheric impacts

6.5.1 Overview

Climate models are a vital tool to help understand and describe the dynamical and chemical response to the Hunga volcanic eruption. As such, the Hunga volcanic eruption is an excellent natural testbed for general model performance, and careful interpretation of the results could provide vital guidance on how to improve such models.

In this section, we describe the upper-atmospheric results of the Hunga Tonga-Hunga Ha'Pai Model Observations Comparison (HTHH-MOC, Zhu et al., 2025), experiment 1. We include only models which have a fully-resolved mesosphere, i.e. WACCM6/MAM (Mills et al., 2016; Zhu et al., 2022), GSFC2D (Fleming et al., 2020; Fleming et al., 2024), and CMAM (Jonsson et al., 2004; Scinocca et al., 2008). WACCM has both required fixed-SST and additional optional coupled ocean settings, with 30 ensemble members and both H$_2$O and SO$_2$ injection in the two settings. CMAM has 10 ensemble members with fixed SST fields and with H$_2$O injection only. GSFC2D has 10 ensemble members with fixed SST fields and with H$_2$O injection only for 5 years, and additional 20 ensemble members with both H$_2$O and SO$_2$ injection but runs 2 years. We use the GSFC2D H2O only ensemble to check the long-term evaluation of the field in Section 6.5.2 and 6.5.3, and use the H$_2$O and SO$_2$ ensemble to check the dynamics response in Section 6.5.4. More details of HTHH-MOC data analysis related to Chapter 6 can be found in Supplementary S3 PartS3.5.

6.5.2 Water vapour plume in the mesosphere

The mesospheric water vapour burden anomaly reached 2 Tg by May 2023, peaking at 3.3 Tg in November 2023. For context, Feofilov et al. (2009) estimated that the normal mesospheric water vapour burden (between 1 hPa and 0.01 hPa) lies in the range 17–21 Tg, implying an approximate 16% increase in total mesospheric water vapour burden (Figure 6.4a). This multi-model mean is comparable to, though some-
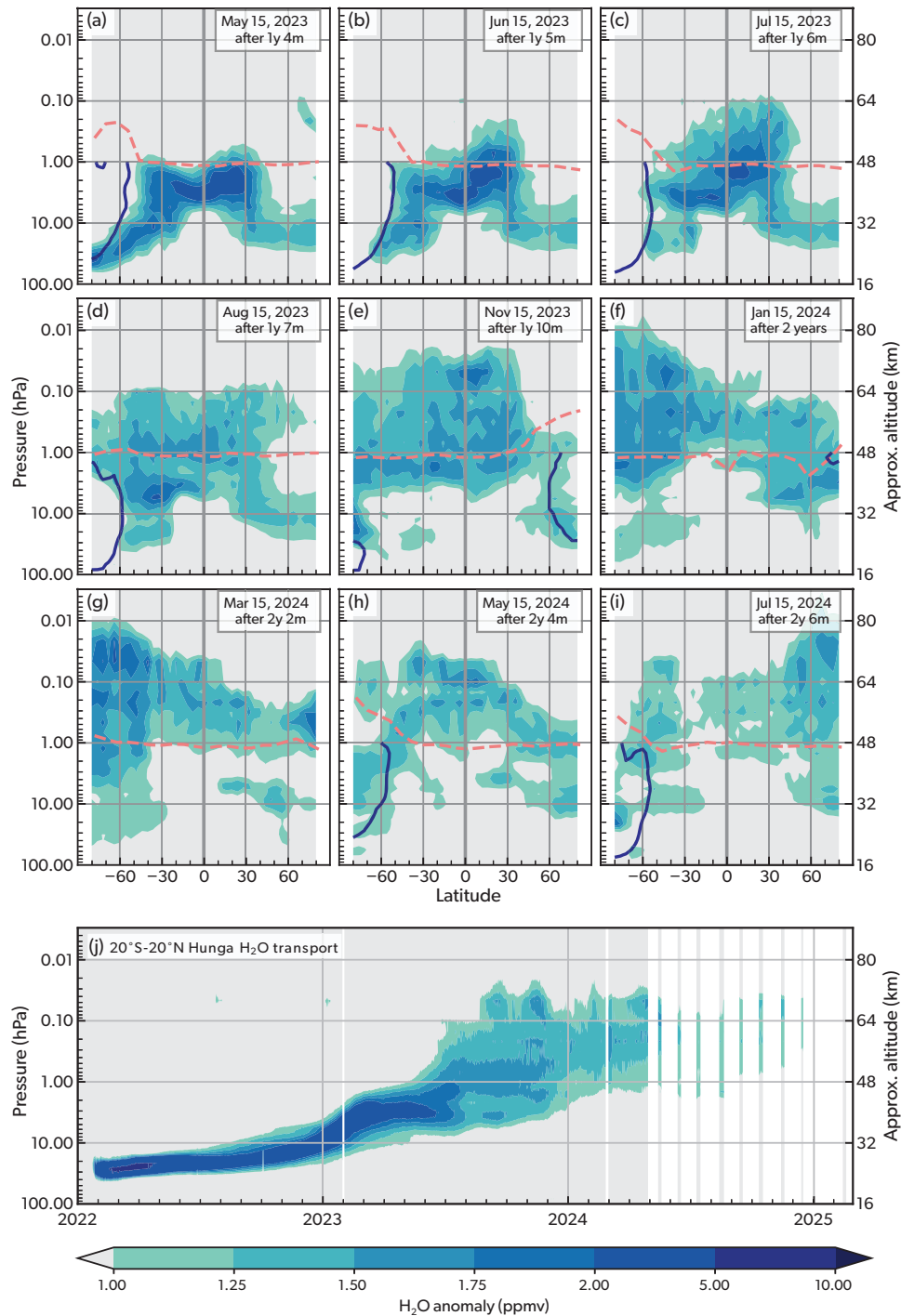
Figure 6.2: *(a–i) Daily zonal-mean water vapour anomalies measured by MLS relative to the 2005–2021 climatology for each day. The stratopause, as determined from MLS temperature measurements, is represented by dashed pink lines. Dark blue lines show contours of scaled potential vorticity (see, e.g., Dunkerton and Delisi, 1986; Manney et al., 1994) approximating the stratospheric polar vortex edge region. Adapted from Millán et al. (2024). (j) Zonal-mean tropical (20°S–20°N) anomalies displaying the Hunga transport through the Brewer−Dobson circulation, demonstrating that water vapour injected by the plume reached the mesosphere (i.e., ~1 hPa) around May 2023.*
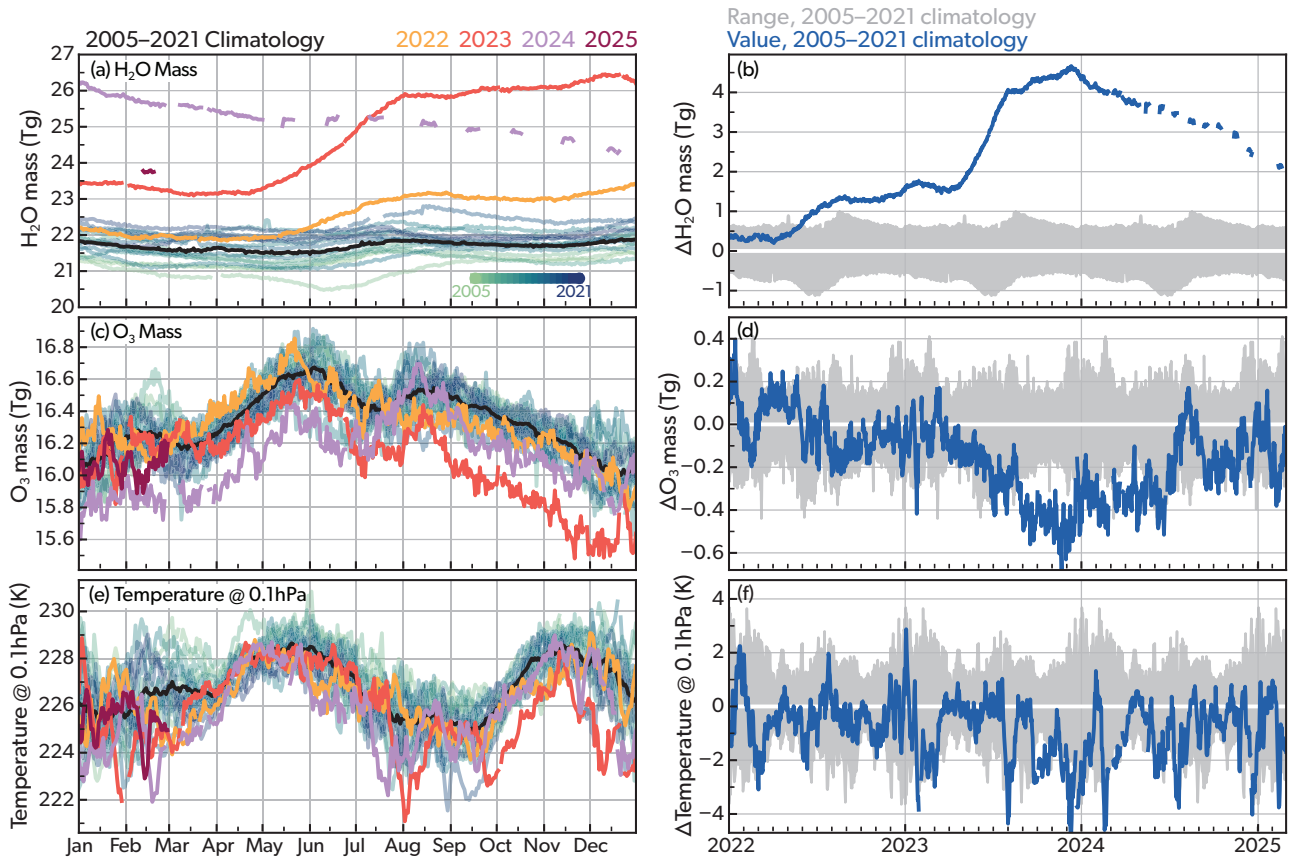
Figure 6.3: *MLS-derived estimates (left side) of the evolution of the (a) global [82°S-82°N] mesospheric [1−0.01 hPa] water vapour burden, (c) global mesospheric ozone burden, (e) mid-mesospheric [0.1 hPa] temperature. The right side shows the same variables, but with the annual cycle removed.*

what lower than, the anomaly estimated from MLS observations (Figure 6.4a; cf. Section 6.4).

The multi-model mean of the runs clearly shows evidence of the Hunga-injected water vapour plume starting to enter the mesosphere following the eruption. The water vapour burden anomaly reached 2 Tg by May 2023, with a maximum of 3.30 Tg reached in November 2023. For context, Feofilov et al. (2009) estimate the normal mesospheric water vapour burden as between 1 hPa and 0.01 hPa as lying in the range 17−21 Tg, and thus this represents an 16% increase in the total mesospheric water vapour burden (Figure 6.4a). This multi-model mean is reasonably comparable to but lower than the anomaly calculated from MLS (Figure 6.4a; cf. Section 6.4). From November 2023 the injected water vapour began to descend, and by the end of 2026, 0.63 Tg of injected water vapour remained in the mesosphere, accounting for 3% of the total mesospheric water vapour burden (Figure 6.4a).

In general, the model results exhibit only relatively small variations in the water vapour plume and match observations well (Figure 6.4a). GSFC2D shows the highest water vapour burden anomaly at 4.07 Tg, with the other models' maximum water vapour burden lying in the range 3.1-3.3 Tg. When interpreting these results, it is important to remember that the water vapour burden anomaly as calculated from the models is defined as the difference between the volcanic and control runs, while for the observations it is defined as the difference from climatology and thus includes natural variability. In temporal terms, the maximum water vapour burden in the GSFC2D ocean run agrees well with the observations and with the multi model mean, 1-2 months early in WACCM and multi-model mean, and 3-4. All models predict a water vapour burden anomaly lower than 1 Tg by the end of 2026.

6.5.3 Mesospheric cooling in 2023

The water vapour plume had a net radiative cooling effect (cross cf. Chapter 4). Additionally, in 2023 after the Hunga-associated water vapour entered the mesosphere, additional HOx reactions led to the depletion of mesospheric ozone, which combined with the water vapour related cooling to produce a >1 K decrease in the global mean mesospheric temperature (Randel
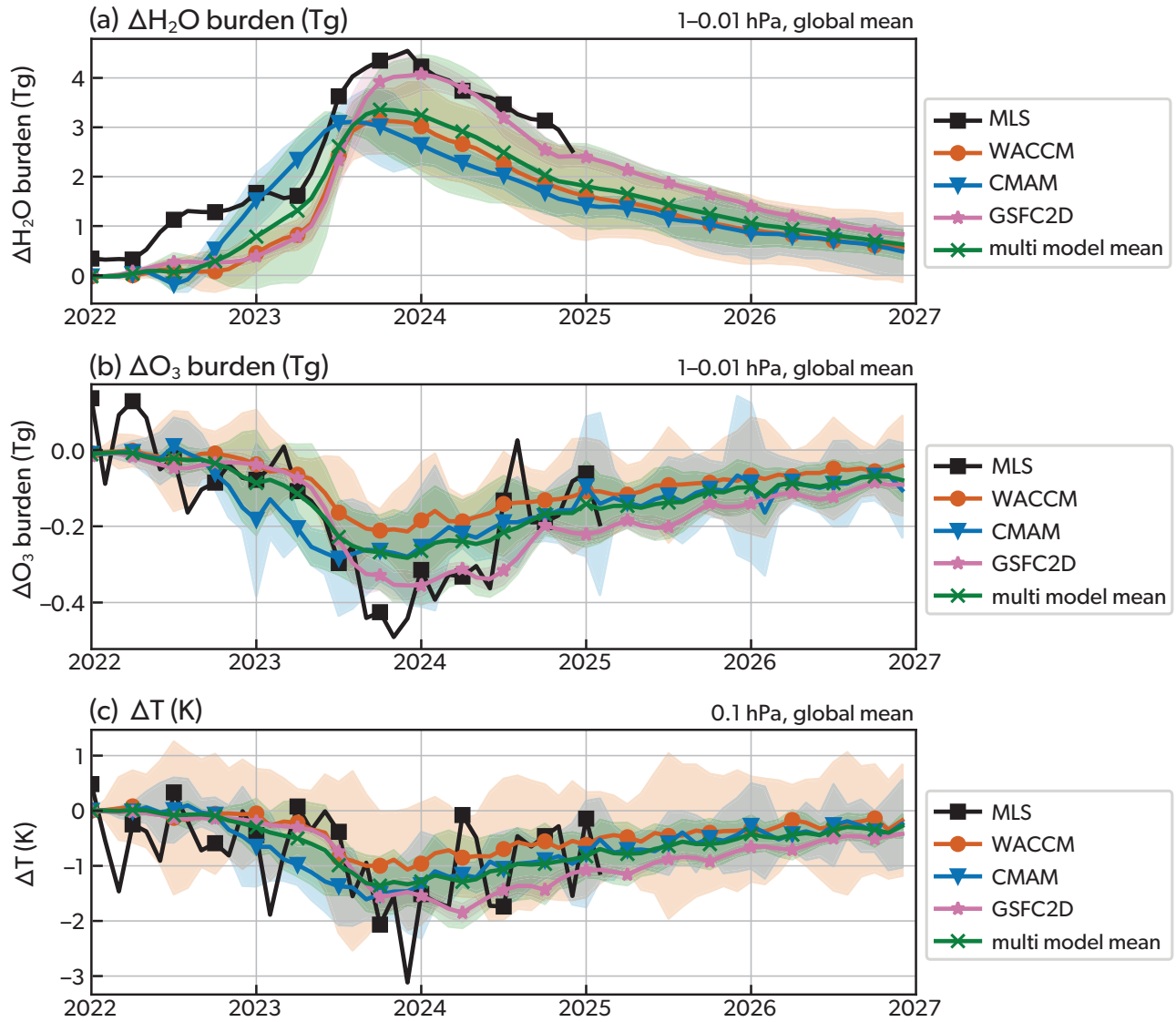
Figure 6.4: *Anomalies of (a) mesospheric water vapour burden and (b) mesospheric ozone burden, observed by (black) MLS, and as differences between the volcanic case and the control case in the (yellow) WACCM-coupled ocean, (pink) WACCM-fixed SST, (blue) CMAM, and (orange) GSFC2D models, and as (green) a multi model mean. Shading denotes the range within 1 standard deviation of the mean.*

et al., 2024).

Our model results are consistent with the changes of ozone and temperature described by Randel et al. (2024). The multi-model-mean global-mean ozone burden started to significantly decrease in 2023 after the water vapour plume entered the mesosphere, and almost simultaneously the mesospheric temperature began to decrease in response to the ozone depletion (Figure 6.5). In general, all models capture the cooling and the ozone depletion, and the model-to-model variation of ozone follows the variation of the water vapour burden in the models (Figure 6.4b).

6.5.4 Mesospheric circulation and temperature response in 2022

One of the most important mesospheric responses to the Hunga volcanic eruption was a large change in temperature. This was observed by the Sounding of the Atmosphere using Broadband Emission Radiometry (SABER) instrument during boreal summer 2022, which saw record-breaking warming over the southern hemisphere extra tropics and cooling throughout of the rest parts of the mesosphere (Yu et al., 2023, Figure 6.6a). Results from WACCM suggest that this was a response to the record-breaking stronger stratospheric westerlies after the eruption (cross cf. Chapter 4). These stronger stratospheric
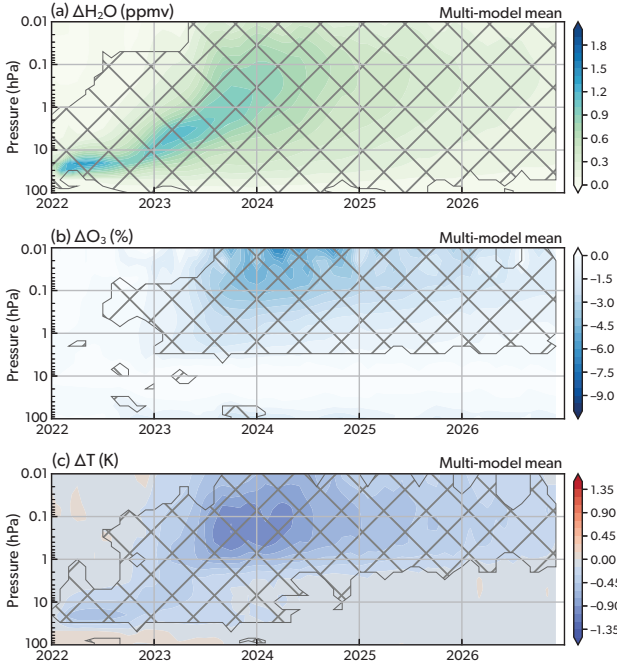
Figure 6.5: *Multi-model mean global differences in (a) water vapour (ppmv), (b) ozone (in percentage), and (c) temperature (K) between the volcanic case (H_2O and SO_2 in WACCM, or H_2O only in CMAM and GSFC2D) and the control case. Areas with hatching indicate statistically significant differences.*

Figure 6.6: *Zonal mean temperature differences between the volcanic case (H_2O and SO_2 in WACCM and GSFC2D, or H_2O only in CMAM) and the control case in July-August 2022, (a) as observed by SABER and adapted from Yu et al. (2023), and as simulated in the (b) WACCM, (c) CMAM, and (d) GSFC2D models. Areas with hatching indicate statistically significant differences.*

westerlies enhanced westward gravity wave drag in the mesosphere, resulting in a 20% stronger mesospheric meridional circulation, and corresponding record-breaking temperature variations (Yu et al., 2023). This temperature response in 2022 was an indirect impact of Hunga's dynamically-driven water injection, as it occurred prior to the appearance of water anomalies in the mesosphere in 2023.

However, it has turned out to be technically challenging to reproduce this dynamical process in models. The response in this model is statistically significant in the WACCM, which has 60 ensemble members that can better disentangle the Hunga dynamics forcing and the internal variability. However, the magnitude of the response of WACCM is much smaller than the observed anomaly. It is of correct sign but not significant in CMAM, with almost no response seen in GSFC2D. The very small response in GSFC2D is likely due to concomitantly small internal variability, as dynamical responses in the model are driven by a combination of radiative forcing and tropospheric planetary and gravity wave forcing which are the same for the control and Hunga perturbation simulations. The resulting circulation and dynamically induced temperature responses are weak compared to 3D models which have much larger internal vari-
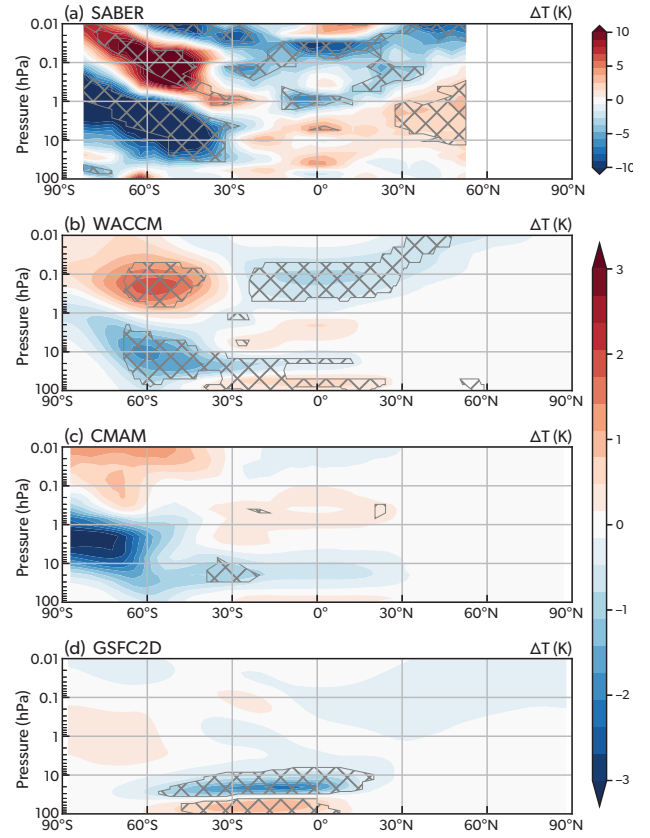
ability. These unpromising model simulation results are consistent with the idea that the response was to some degree stochastic in nature (Yu et al., 2023).

6.6 Summary

The Hunga eruption of 2022 had profound short-term dynamical impacts on the middle and upper atmosphere. The initial explosion triggered a complex array of Lamb, acoustic, and gravity waves that propagated rapidly from the surface to the thermosphere and ionosphere and transversed the globe several times, demonstrating strong and direct dynamical coupling across the depth of the atmosphere. The eruption's short- and long-term influences extended into both the neutral thermosphere and charged ionosphere, generating disturbances including MSTIDs and LSTIDs and causing significant ionospheric depletion and electric field disturbances. MSTIDs were also observed in the magnetic conjugate location to the

eruptive wave release (Lin et al., 2022). These effects highlight the complex coupling mechanisms between atmospheric layers and the geomagnetic environment and may have important research implications for applied topics such as tsunami warning systems as well as into fundamental aspects of atmospheric science theory.

Chemically, the eruption injected substantial water vapour into the stratosphere, which was then transported into the mesosphere during 2023 via the Brewer-Dobson circulation, leading to mesospheric cooling and ozone depletion via HOx chemistry and radiative processes. Dynamically, the Hunga eruption caused strong stratospheric westerlies in 2022 and enhanced westward gravity wave drag in the mesosphere, leading to record-breaking warming over the Southern hemisphere extra tropics and cooling throughout the rest of the mesosphere during boreal summer 2022. Climate models have subsequently been employed to simulate these effects, with varying degrees of success. Models are able to reproduce the mesospheric water vapour, ozone and cooling responses well. The response reached a maximum in late 2023, then gradually diminished and is expected to return to its pre-eruption state in 2027. Only the ocean-coupled climate model showed the significant dynamical and temperature response observed in summer 2022.

It is important to note that the impact of this water vapour operates at long timescales, and is still ongoing at time of writing, and thus we are not able to fully describe all upper-atmospheric impacts in this report. However, results at time of writing suggest that the models generally captured the water vapour transport and its direct impact on mesospheric temperature and ozone, but have had challenges in reproducing dynamical processes. This highlights the complexity of the eruption's influence on the middle and upper atmospheric system and the nonlinear chemical and dynamical interactions driven by the eruption.

References

Aa, E., S.-R. Zhang, P. J. Erickson, J. Vierinen, A. J. Coster, L. P. Goncharenko, A. Spicher and W. Rideout (2022a). 'Significant Ionospheric Hole and Equatorial Plasma Bubbles After the 2022 Tonga Volcano Eruption'. *Space Weather*, 20, e2022SW003101. DOI: 10.1029/2022SW003101.

Aa, E., S.-R. Zhang, W. Wang, P. J. Erickson, L. Qian, R. Eastes, B. J. Harding, T. J. Immel, D. K. Karan, R. E. Daniell et al. (2022b). 'Pronounced Suppression and X-Pattern Merging of Equatorial Ionization Anomalies After the 2022 Tonga Volcano Eruption'. *J. Geophys. Res.*, 127, e2022JA030527. DOI: 10.1029/2022ja030527.

Aryal, S., Q. Gan, J. S. Evans, F. I. Laskar, D. K. Karan, X. Cai, K. R. Greer, W. Wang, W. E. McClintock and R. W. Eastes (2023). 'Tongan Volcanic Eruption Induced Global-Scale Thermospheric Changes Observed by the GOLD Mission'. *Geophys. Res. Lett.*, 50, e2023GL103158. DOI: 10.1029/2023gl103158.

Astafyeva, E., B. Maletckii, T. D. Mikesell, E. Munaibari, M. Ravanelli, P. Coisson, F. Manta and L. Rolland (2022). 'The 15 January 2022 Hunga Tonga Eruption History as Inferred From Ionospheric Observations'. *Geophys. Res. Lett.*, 49, e2022GL098827. DOI: 10.1029/2022GL098827.

Brasseur, G. P. and S. Solomon (2005). *Aeronomy of the middle atmosphere.* Dordrecht, The Netherlands: Springer.

Carr, J. L., Á. Horváth, D. L. Wu and M. D. Friberg (2022). 'Stereo Plume Height and Motion Retrievals for the Record-Setting Hunga Tonga-Hunga Ha'apai Eruption of 15 January 2022'. *Geophys. Res. Lett.*, 49, e2022GL098131. DOI: 10.1029/2022gl098131.

Carter, B. A., R. Pradipta, T. Dao, J. L. Currie, S. Choy, P. Wilkinson et al. (2023). 'The ionospheric effects of the 2022 Hunga Tonga volcano eruption and the associated impacts on GPS precise point positioning across the Australian region'. *Space Weather*, 21, e2023SW003476. DOI: 10.1029/2023SW003476.

Chau, J. L., F. L. Poblet, H.-L. Liu, A. Liu, N. Gulbrandsen, C. Jacobi, R. R. Rodriguez, D. Scipion and M. Tsutsumi (2024). 'Mesosphere and lower thermosphere wind perturbations due to the 2022 Hunga Tonga–Hunga Ha'apai eruption as observed by multistatic specular meteor radars'. *Radio Sci.*, 59. DOI: 10.1029/2024RS008013.

Choi, J. M., C. C. H. Lin, P. K. Rajesh et al. (2023). 'Giant ionospheric density hole near the 2022 Hunga–Tonga volcanic eruption: Multi-point satellite ob-servations'. *Earth Planets Space*, 75, 184. DOI: 10.1186/s40623-023-01933-1.

Dunkerton, T. J. and D. P. Delisi (1986). 'Evolution of potential vorticity in the winter stratosphere of January–February 1979'. *J. Geophys. Res.*, 91, pp. 1199–1208. DOI: 10.1029/JD091iD01p01199.

Ern, M., L. Hoffmann, S. Rhode and P. Preusse (2022). 'The mesoscale gravity wave response to the 2022 Tonga volcanic eruption: AIRS and MLS satellite observations and source backtracing'. *Geophys. Res. Lett.*, 49, e2022GL098626. DOI: 10.1029/2022GL098626.

Feofilov, A. G., A. A. Kutepov, W. D. Pesnell, R. A. Goldberg, B. T. Marshall, L. L. Gordley and J. M. I. Russell (2009). 'Daytime SABER/TIMED observations of water vapor in the mesosphere: Retrieval approach and first results'. *Atmos. Chem. Phys.*, 9, pp. 8139–8158. DOI: 10.5194/acp-9-8139-2009.

Figueiredo, C. A. O. B., S. L. Vadas, E. Becker, C. M. Wrasse, H. Takahashi, P. K. Nyassor and D. Barros (2023). 'Secondary gravity waves from the Tonga volcano eruption: Observation and modeling over New Zealand and Australia'. *J. Geophys. Res.*, 128, e2023JA031476. DOI: 10.1029/2023JA031476.

Fleming, E. L., P. A. Newman, Q. Liang and J. S. Daniel (2020). 'The Impact of Continuing CFC-11 Emissions on Stratospheric Ozone'. *J. Geophys. Res.*, 125, e2019JD031849. DOI: 10.1029/2019jd031849.

Fleming, E. L., P. A. Newman, Q. Liang and L. D. Oman (2024). 'Stratospheric Temperature and Ozone Impacts of the Hunga Tonga-Hunga Ha'apai Water Vapor Injection'. *J. Geophys. Res.*, 129, e2023JD039298. DOI: 10.1029/2023jd039298.

Gasque, L. C., Y.-J. Wu, B. J. Harding, T. J. Immel and C. C. Triplett (2022). 'Rapid volcanic modification of the E-region dynamo: ICON's first glimpse of the Tonga eruption'. *Geophys. Res. Lett.*, 49, e2022GL100825. DOI: 10.1029/2022GL100825.

Han, S.-C., S. McClusky, T. D. Mikesell, L. Rolland, E. Okal and C. Benson (2023). 'CubeSat GPS observation of traveling ionospheric disturbances after the 2022 Hunga–Tonga Hunga–Ha'apai volcanic eruption and its potential use for tsunami warning'. *Earth Space Sci.*, 10, e2022EA002586. DOI: 10.1029/2022EA002586.

Harding, B. J., Y.-J. J. Wu, P. Alken, Y. Yamazaki, C. C. Triplett, T. J. Immel, L. C. Gasque, S. B. Mende and C. Xiong (2022). 'Impacts of the January 2022 Tonga volcanic eruption on the ionospheric dynamo: ICON–MIGHTI and Swarm observations of extreme neutral winds and currents'. *Geophys. Res.*

Lett., 49, e2022GL098577. DOI: `10.1029/2022GL09` `8577`.

He, J., E. Astafyeva, X. Yue, F. Ding and B. Maletckii (2023). 'The giant ionospheric depletion on 15 January 2022 around the Hunga Tonga–Hunga Ha'apai volcanic eruption'. *J. Geophys. Res.*, 128, e2022JA030984. DOI: `10.1029/2022JA030984`.

Huba, J. D., E. Becker and S. L. Vadas (2023). 'Simulation study of the 15 January 2022 Tonga event: Development of super equatorial plasma bubbles'. *Geophys. Res. Lett.*, 50, e2022GL101185. DOI: `10.10` `29/2022GL101185`.

Inchin, P. A., A. Bhatt, S. A. Cummer, S. D. Eckermann, B. J. Harding, D. D. Kuhl, J. Ma, J. J. Makela, R. Sabatini and J. B. Snively (2023). 'Multi-layer evolution of acoustic-gravity waves and ionospheric disturbances over the United States after the 2022 Hunga Tonga volcano eruption'. *AGU Adv.*, 4, e2023AV000870. DOI: `10.1029/2023AV000870`.

Jonsson, A. I., J. de Grandpré, V. I. Fomichev, J. C. McConnell and S. R. Beagley (2004). 'Doubled CO2-induced cooling in the middle atmosphere: Photochemical analysis of the ozone radiative feedback'. *J. Geophys. Res.*, 109, D24103. DOI: `10.1029/2004` `JD005093`.

Klenzing, J., K. Zawdie, E. Astafyeva, A. Belehaki, M. Burleigh, A. G. Burrell, C. A. O. B. Figueiredo, N. A. Frissell, W. Fu, D. Hickey et al. (2025). 'Resolving the generation mechanisms and electrodynamical effects of medium-scale traveling ionospheric disturbances (MSTIDs)'. *Front. Astron. Space Sci.*, 12, 1539821. DOI: `10.3389/fspas.2025.1539821`.

Lamb, H. (1881). 'On the vibrations of an elastic sphere'. *Proc. Lond. Math. Soc.*, s1-13, pp. 189–212. DOI: `10.1112/plms/s1-13.1.189`.

Landerer, F. W., F. M. Flechtner, H. Save, F. H. Webb, T. Bandikova, W. I. Bertiger, S. V. Bettadpur, S. H. Byun, C. Dahle, H. Dobslaw et al. (2020). 'Extending the global mass change data record: GRACE Follow-On instrument and science data performance'. *Geophys. Res. Lett.*, 47, e2020GL088306. DOI: `10.1029/2020GL088306`.

Le, G., G. Liu, E. Yizengaw and C. R. Englert (2022). 'Intense equatorial electrojet and counter electrojet caused by the 15 January 2022 Tonga volcanic eruption: Space- and ground-based observations'. *Geophys. Res. Lett.*, 49, e2022GL099002. DOI: `10.10` `29/2022GL099002`.

Lee, Y.-K., N. Hindley, C. Grassotti and Q. Liu (2023). 'The Hunga Tonga–Hunga Ha'apai volcanic eruption as seen in satellite microwave observations and

MiRS temperature retrievals'. *Geophys. Res. Lett.*, 50, e2023GL106439. DOI: `10.1029/2023GL106439`.

Legras, B., C. Duchamp, P. Sellitto, A. Podglajen, E. Carboni, R. Siddans, J.-U. Grooß, S. Khaykin and F. Ploeger (2022). 'The evolution and dynamics of the Hunga Tonga–Hunga Ha'apai sulfate aerosol plume in the stratosphere'. *Atmos. Chem. Phys.*, 22, pp. 14957–14970. DOI: `10.5194/acp-22-14957-2` `022`.

Leslie, R. C. (1885). 'Sky glows'. *Nature*, 32, 245. DOI: `10.1038/032245a0`.

Li, R., J. Lei, J. Kusche, T. Dang, F. Huang, X. Luan, S.-R. Zhang, M. Yan, Z. Yang, F. Liu et al. (2023a). 'Large-scale disturbances in the upper thermosphere induced by the 2022 Tonga volcanic eruption'. *Geophys. Res. Lett.*, 50, e2022GL102265. DOI: `10.1029` `/2022GL102265`.

Li, X., F. Ding, X. Yue, T. Mao, B. Xiong and Q. Song (2023b). 'Multiwave structure of traveling ionospheric disturbances excited by the Tonga volcanic eruptions observed by a dense GNSS network in China'. *Space Weather*, 21, e2022SW003210. DOI: `10.1029/2022SW003210`.

Lin, J.-T., P. K. Rajesh, C. C. H. Lin, M.-Y. Chou, J.-Y. Liu, J. Yue, T.-Y. Hsiao, H.-F. Tsai, H.-M. Chao and M.-M. Kung (2022). 'Rapid conjugate appearance of the giant ionospheric Lamb wave signatures in the northern hemisphere after Hunga Tonga volcano eruptions'. *Geophys. Res. Lett.*, 49, e2022GL098222. DOI: `10.1029/2022GL098222`.

Liu, C. H., J. Klostermeyer, K. C. Yeh, T. B. Jones, T. Robinson, O. Holt, R. Leitinger, T. Ogawa, K. Sinno, S. Kato et al. (1982). 'Global dynamic responses of the atmosphere to the eruption of Mount St. Helens on May 18, 1980'. *J. Geophys. Res.*, 87, pp. 6281–6290. DOI: `10.1029/JA087iA08p06281`.

Liu, H.-L., W. Wang, J. D. Huba, P. H. Lauritzen and F. Vitt (2023). 'Atmospheric and ionospheric responses to the Hunga–Tonga volcano eruption simulated by WACCM-X'. *Geophys. Res. Lett.*, 50, e2023GL103682. DOI: `10.1029/2023GL103682`.

Liu, X., J. Xu, J. Yue and M. Kogure (2022). 'Strong gravity waves associated with the Tonga volcano eruption revealed by SABER observations'. *Geophys. Res. Lett.*, 49, e2022GL098339. DOI: `10.1029` `/2022GL098339`.

Maletckii, B. and E. Astafyeva (2022). 'Near-real-time analysis of the ionospheric response to the 15 January 2022 Hunga Tonga–Hunga Ha'apai volcanic eruption'. *J. Geophys. Res.*, 127, e2022JA030735. DOI: `10.1029/2022JA030735`.

Manney, G. L., R. W. Zurek, M. E. Gelman, A. J. Miller and R. Nagatani (1994). 'The anomalous Arctic lower stratospheric polar vortex of 1992–1993'. *Geophys. Res. Lett.*, 21, pp. 2405–2408. DOI: `10.1029/94gl02368`.

Matoza, R. S., D. Fee, J. D. Assink, A. M. Iezzi, D. N. Green, K. Kim, L. Toney, T. Lecocq, S. Krishnamoorthy, J.-M. Lalande et al. (2022). 'Atmospheric waves and global seismoacoustic observations of the January 2022 Hunga eruption, Tonga'. *Science*, 377, pp. 95–100. DOI: `10.1126/science.abo7063`.

Millán, L., W. G. Read, M. L. Santee, A. Lambert, G. L. Manney, J. L. Neu, M. C. Pitts, F. Werner, N. J. Livesey and M. J. Schwartz (2024). 'The Evolution of the Hunga Hydration in a Moistening Stratosphere'. *Geophys. Res. Lett.*, 51, e2024GL110841. DOI: `10.1029/2024gl110841`.

Millán, L., M. L. Santee, A. Lambert, N. J. Livesey, F. Werner, M. J. Schwartz, H. C. Pumphrey, G. L. Manney, Y. Wang, H. Su et al. (2022). 'The Hunga Tonga-Hunga Ha'apai Hydration of the Stratosphere'. *Geophys. Res. Lett.*, 49, e2022GL099381. DOI: `10.1029/2022gl099381`.

Miller, S. D., W. C. Straka, J. Yue, S. M. Smith, M. J. Alexander, L. Hoffmann, M. Setvák and P. T. Partain (2015). 'Upper atmospheric gravity wave details revealed in nightglow satellite imagery'. *Proc. Natl. Acad. Sci. U.S.A.*, 112, E6728–E6735. DOI: `10.1073/pnas.1508084112`.

Mills, M. J., A. Schmidt, R. Easter, S. Solomon, D. E. Kinnison, S. J. Ghan et al. (2016). 'Global volcanic aerosol properties derived from emissions, 1990–2014, using CESM1 (WACCM)'. *J. Geophys. Res.*, 121, pp. 2332–2348. DOI: `10.1002/2015jd024290`.

Miyoshi, Y. and H. Shinagawa (2023). 'Upward propagation of gravity waves and ionospheric perturbations triggered by the 2022 Hunga–Tonga volcanic eruption'. *Earth Planets Space*, 75, 68. DOI: `10.1186/s40623-023-01827-2`.

Nedoluha, G. E., R. M. Gomez, I. Boyd, H. Neal, D. R. Allen and A. Lambert (2024). 'The Spread of the Hunga Tonga H2O Plume in the Middle Atmosphere Over the First Two Years Since Eruption'. *J. Geophys. Res.*, 129, e2024JD040907. DOI: `10.1029/2024jd040907`.

Nedoluha, G. E., R. M. Gomez, I. Boyd, H. Neal, D. R. Allen, A. Lambert and N. J. Livesey (2023). 'Mesospheric Water Vapor in 2022'. *J. Geophys. Res.*, 128, e2023JD039196. DOI: `10.1029/2023jd039196`.

Niemeier, U., S. Wallis, C. Timmreck, T. van Pham and C. von Savigny (2023). 'How the Hunga Tonga—Hunga Ha'apai Water Vapor Cloud Impacts Its Transport Through the Stratosphere: Dynamical and Radiative Effects'. *Geophys. Res. Lett.*, 50, e2023GL106482. DOI: `10.1029/2023gl106482`.

Ohya, H., F. Tsuchiya, T. Takamura, H. Shinagawa, Y. Takahashi and A. B. Chen (2024). 'Lower ionospheric resonance caused by Pekeris wave induced by the 2022 Tonga volcanic eruption'. *Sci. Rep.*, 14, 15659. DOI: `10.1038/s41598-024-65929-x`.

Pacheco, E. E., J. P. Velasquez, R. Flores, L. Condori, G. Fajardo, K. Kuyeng, D. E. Scipion, M. Milla, J. F. Conte, F. L. Poblet et al. (2024). 'The impact of the Hunga Tonga–Hunga Ha'apai volcanic eruption on the Peruvian atmosphere: From the sea surface to the ionosphere'. *Earth Planets Space*, 76, 79. DOI: `10.1186/s40623-024-02022-7`.

Poblet, F. L., J. L. Chau, J. F. Conte, J. Vierinen, J. Suclupe, A. Liu and R. R. Rodriguez (2023). 'Extreme horizontal wind perturbations in the mesosphere and lower thermosphere over South America associated with the 2022 Hunga eruption'. *Geophys. Res. Lett.*, 50, e2023GL103809. DOI: `10.1029/2023GL103809`.

Pradipta, R., B. A. Carter, J. L. Currie, S. Choy, P. Wilkinson, P. Maher and R. Marshall (2023). 'On the propagation of traveling ionospheric disturbances from the Hunga Tonga–Hunga Ha'apai volcano eruption and their possible connection with tsunami waves'. *Geophys. Res. Lett.*, 50, e2022GL101925. DOI: `10.1029/2022GL101925`.

Proud, S. R., A. T. Prata and S. Schmauß (2022). 'The January 2022 eruption of Hunga Tonga-Hunga Ha'apai volcano reached the mesosphere'. *Science*, 378, pp. 554–557. DOI: `10.1126/science.abo4076`.

Rajesh, P. K., C. C. H. Lin, J. T. Lin, C. Y. Lin, J. Y. Liu, T. Matsuo, C. Y. Huang, M. Y. Chou, J. Yue, M. Nishioka et al. (2022). 'Extreme poleward expanding super plasma bubbles over the Asia–Pacific region triggered by the Tonga volcano eruption during the recovery phase of a geomagnetic storm'. *Geophys. Res. Lett.*, 49, e2022GL099798. DOI: `10.1029/2022GL099798`.

Randel, W. J., X. Wang, J. Starr, R. R. Garcia and D. Kinnison (2024). 'Long-Term Temperature Impacts of the Hunga Volcanic Eruption in the Stratosphere and Above'. *Geophys. Res. Lett.*, 51. DOI: `10.1029/2024gl111500`.

Ravanelli, M., E. Astafyeva, E. Munaibari, L. Rolland and T. D. Mikesell (2023). 'Ocean–ionosphere disturbances due to the 15 January 2022 Hunga Tonga–Hunga Ha'apai eruption'. *Geophys. Res. Lett.*, 50, e2022GL101465. DOI: `10.1029/2022GL101465`.

Scinocca, J. F., N. A. McFarlane, M. Lazare, J. Li and D. Plummer (2008). 'Technical Note: The CCCma third generation AGCM and its extension into the middle atmosphere'. *Atmos. Chem. Phys.*, 8, pp. 7055–7074. DOI: `10.5194/acp-8-7055-2008`.

Sellitto, P., A. Podglajen, R. Belhadji, M. Boichu, E. Carboni, J. Cuesta, C. Duchamp, C. Kloss, R. Siddans, N. Bègue et al. (2022). 'The unexpected radiative impact of the Hunga Tonga eruption of 15th January 2022'. *Commun. Earth Environ.*, 3, 288. DOI: `10.1038/s43247-022-00618-z`.

Sepúlveda, I., M. Carvajal and D. C. Agnew (2023). 'Global Winds Shape Planetary-Scale Lamb Waves'. *Geophys. Res. Lett.*, 50, e2023GL106097. DOI: `10.1029/2023GL106097`.

Shinbori, A., Y. Otsuka, T. Sori, M. Nishioka, S. Perwitasari, T. Tsuda et al. (2022). 'Electromagnetic conjugacy of ionospheric disturbances after the 2022 Hunga Tonga–Hunga Ha'apai volcanic eruption as seen in GNSS–TEC and SuperDARN Hokkaido pair of radars observations'. *Earth Planets Space*, 74, 106. DOI: `10.1186/s40623-022-01665-8`.

Shinbori, A., T. Sori, Y. Otsuka, M. Nishioka, S. Perwitasari, T. Tsuda et al. (2023). 'Generation of equatorial plasma bubble after the 2022 Tonga volcanic eruption'. *Sci. Rep.*, 13, 6450. DOI: `10.1038/s41598-023-33603-3`.

Smart, D. (2022). 'The first hour of the paroxysmal phase of the 2022 Hunga Tonga–Hunga Ha'apai volcanic eruption as seen by a geostationary meteorological satellite'. *Weather*, 77, pp. 81–82. DOI: `10.1002/wea.4173`.

Stober, G., A. Liu, A. Kozlovsky, Z. Qiao, W. Krochin, G. Shi, J. Kero, M. Tsutsumi, N. Gulbrandsen, S. Nozawa et al. (2023). 'Identifying gravity waves launched by the Hunga Tonga–Hunga Ha'apai volcanic eruption in mesosphere/lower-thermosphere winds derived from CONDOR and the Nordic Meteor Radar Cluster'. *Ann. Geophys.*, 41, pp. 197–208. DOI: `10.5194/angeo-41-197-2023`.

Stober, G., S. L. Vadas, E. Becker, A. Liu, A. Kozlovsky, D. Janches, Z. Qiao, W. Krochin, G. Shi, W. Yi et al. (2024). 'Gravity waves generated by the Hunga Tonga–Hunga Ha'apai volcanic eruption and their global propagation in the mesosphere/lower thermosphere observed by meteor radars and modeled with the High-Altitude general Mechanistic Circulation Model'. *Atmos. Chem. Phys.*, 24, pp. 4851–4873. DOI: `10.5194/acp-24-4851-2024`.

Takahashi, H., C. A. O. B. Figueiredo, D. Barros, C. M. Wrasse, G. A. Giongo, R. H. Honda, L. F. R. Vital, L. C. A. Resende, P. K. Nyassor, T. T. Ayorinde et al. (2023). 'Ionospheric disturbances over South America related to the Tonga volcanic eruption'. *Earth Planets Space*, 75, 92. DOI: `10.1186/s40623-023-01844-1`.

Themens, D. R., C. Watson, N. Žagar, S. Vasylkevych, S. Elvidge, A. McCaffrey, P. Prikryl, B. Reid, A. Wood and P. T. Jayachandran (2022). 'Global propagation of ionospheric disturbances associated with the 2022 Tonga volcanic eruption'. *Geophys. Res. Lett.*, 49, e2022GL098158. DOI: `10.1029/2022GL098158`.

Vadas, S. L., E. Becker, C. Figueiredo, K. Bossert, B. J. Harding and L. C. Gasque (2023a). 'Primary and secondary gravity waves and large-scale wind changes generated by the Tonga volcanic eruption on 15 January 2022: Modeling and comparison with ICON-MIGHTI winds'. *J. Geophys. Res.*, 128, e2022JA031138. DOI: `10.1029/2022JA031138`.

Vadas, S. L., C. Figueiredo, E. Becker, J. D. Huba, D. R. Themens, N. P. Hindley, S. Mrak, I. Galkin and K. Bossert (2023b). 'Traveling ionospheric disturbances induced by the secondary gravity waves from the Tonga eruption on 15 January 2022: Modeling with MESORAC–HIAMCM–SAMI3 and comparison with GPS/TEC and ionosonde data'. *J. Geophys. Res.*, 128, e2023JA031408. DOI: `10.1029/2023JA031408`.

Verhulst, T. G. W., D. Altadill, V. Barta, A. Belehaki, D. Burešová, C. Cesaroni et al. (2022). 'Multi-instrument detection in Europe of ionospheric disturbances caused by the 15 January 2022 eruption of the Hunga volcano'. *J. Space Weather Space Clim.*, 12, 35. DOI: `10.1051/swsc/2022032`.

Wallis, S., M. DeLand and C. von Savigny (2025). 'Did the 2022 Hunga eruption impact the noctilucent cloud season in 2023/24 and 2024?' *Atmos. Chem. Phys.*, 25, pp. 3635–3645. DOI: `10.5194/acp-25-3635-2025`.

Watanabe, S., K. Hamilton, T. Sakazaki and M. Nakano (2022). 'First Detection of the Pekeris Internal Global Atmospheric Resonance: Evidence from the 2022 Tonga Eruption and from Global Reanalysis Data'. *J. Atmos. Sci.*, 79, pp. 3027–3043. DOI: `10.1175/JAS-D-22-0078.1`.

Wright, C. J. (2019). 'Quantifying the global impact of tropical cyclone-associated gravity waves using HIRDLS, MLS, SABER, and IBTrACS data'. *Q. J. R. Meteorol. Soc.*, 145, pp. 3023–3039. DOI: `10.1002/qj.3602`.

Wright, C. J., N. P. Hindley, M. J. Alexander, M. Barlow, L. Hoffmann, C. N. Mitchell, F. Prata, M. Bouillon, J. Carstens, C. Clerbaux et al. (2022). 'Surface-to-space atmospheric waves from Hunga Tonga-Hunga Ha'apai eruption'. *Nature*, 609, pp. 741–746. DOI: `10.1038/s41586-022-05012-5`.

Wu, H., X. Lu, W. Wang and H.-L. Liu (2023). 'Simulation of the propagation and effects of gravity waves generated by the Tonga volcano eruption in the thermosphere and ionosphere using nested-grid TIEGCM'. *J. Geophys. Res.*, 128, e2023JA031354. DOI: `10.1029/2023JA031354`.

Yamazaki, Y., G. Soares and J. Matzka (2022). 'Geomagnetic detection of the atmospheric acoustic resonance at 3.8 mHz during the Hunga Tonga eruption event on 15 January 2022'. *J. Geophys. Res.*, 127, e2022JA030540. DOI: `10.1029/2022JA030540`.

Yu, W., R. Garcia, J. Yue, A. Smith, X. Wang, W. Randel, Z. Qiao, Y. Zhu, V. L. Harvey, S. Tilmes et al. (2023). 'Mesospheric temperature and circulation response to the Hunga Tonga-Hunga-Ha'apai volcanic eruption'. *J. Geophys. Res.*, 128, e2023JD039636. DOI: `10.1029/2023JD039636`.

Yue, J., S. D. Miller, W. C. I. Straka, Y.-J. Noh, M.-Y. Chou, R. Kahn and V. Flower (2022). 'La Soufriere volcanic eruptions launched gravity waves into space'. *Geophys. Res. Lett.*, 49, e2022GL097952. DOI: `10.1029/2022GL097952`.

Zettergren, M. D., J. B. Snively, A. Komjathy and O. P. Verkhoglyadova (2017). 'Nonlinear ionospheric responses to large-amplitude infrasonic–acoustic waves generated by undersea earthquakes'. *J. Geophys. Res.*, 122, pp. 2272–2291. DOI: `10.1002/2016JA023159`.

Zhang, H., F. Wang, J. Li, Y. Duan, C. Zhu and J. He (2022). 'Potential Impact of Tonga Volcano Eruption on Global Mean Surface Air Temperature'. *J. Meteorol. Res.*, 36, pp. 1–5. DOI: `10.1007/s13351-022-2013-6`.

Zhou, L., B. Yan, N. Sun, J. Huang, Q. Liu, C. Grassotti, Y.-K. Lee, W. Straka, J. Niu, A. Huff et al. (2023). 'Observed Atmospheric Features for the 2022 Hunga Tonga Volcanic Eruption from Joint Polar Satellite System Science Data Products'. *Atmosphere*, 14, 263, p. 263. DOI: `10.3390/atmos14020263`.

Zhu, Y., H. Akiyoshi, V. Aquila, E. Asher, E. M. Bednarz, S. Bekki, C. Brühl, A. H. Butler, P. Case, S. Chabrillat et al. (2025). 'Hunga Tonga–Hunga Ha'apai Volcano Impact Model Observation Comparison (HTHH-MOC) project: experiment protocol and model descriptions'. *Geosci. Model Dev.*, 18, pp. 5487–5512. DOI: `10.5194/gmd-18-5487-2025`.

Zhu, Y., C. G. Bardeen, S. Tilmes, M. J. Mills, X. Wang, V. L. Harvey, G. Taha, D. Kinnison, R. W. Portmann, P. Yu et al. (2022). 'Perturbations in stratospheric aerosol evolution due to the water-rich plume of the 2022 Hunga-Tonga eruption'. *Commun. Earth Environ.*, 3, 248. DOI: `10.1038/s43247-022-00580-w`.